Deterioration of graffiti spray paints applied on granite after a decade of natural environment

Article *in* Science of The Total Environment · February 2022

DOI: 10.1016/j.scitotenv.2022.154169

Science of the Total Environment 826 (2022) 154169

Contents lists available at ScienceDirect

Science of the Total Environment

journal homepage: www.elsevier.com/locate/scitotenv

Deterioration of graffiti spray paints applied on granite after a decade of natural environment

J.S. Pozo-Antonio *, T. Rivas, N. González, E.M. Alonso-Villar

CINTECX, GESSMin group, Dpto. de Enxeñaría de Recursos Naturais e Medio Ambiente, Escola de Enxeñaría de Minas e Enerxía, Universidade de Vigo, 36310 Vigo, Spain

HIGHLIGHTS

- Non-metallic alkyd- and a metallic polyethylene- paints on granites exposed to outdoor atmosphere.
- Relationship between physical and chemical changes were not found.
- Physical-mechanical changes (craquelure and paint loss) depended on granite texture.
- Chemical changes were more intense in the red and silver paints.

GRAPHICAL ABSTRACT

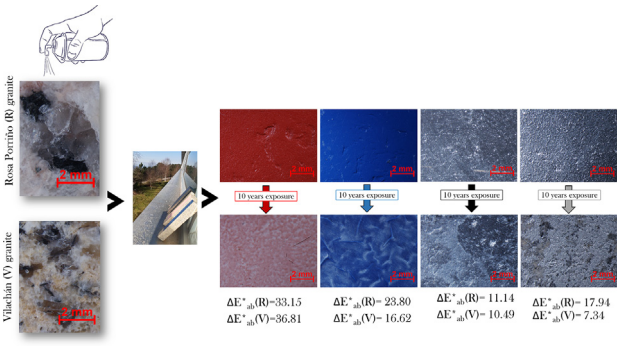

ARTICLE INFO

Article history:
Received 2 November 2021
Received in revised form 12 February 2022
Accepted 23 February 2022
Available online xxxx

Editor: Philip K. Hopke

Keywords:
Graffiti paint
Natural ageing
Physical change
Chemical change
Alkyd paint
Polyethylene paint

ABSTRACT

Graffiti spray paints are commonly used in contemporaneous mural paintings in public spaces, contributing to the transformation of sites and urban life. These outdoor artworks are now beginning to show different deterioration forms, such as physical-mechanical alteration (loss of material and cohesion, etc.) and chromatic changes. However, the deterioration has not been formally characterized, and the influence of the paint composition and underlying substrate are not known. In this study, three non-metallic (red, blue and black) alkyd graffiti spray paints and one metallic (silver) polyethylene graffiti spray paint were applied to two granite stones with different mineralogy and texture and exposed to a natural urban-marine environment near Vigo (NW Spain) for one decade (2010 – 2020). Physical changes were evaluated by stereomicroscopy, colour spectrophotometry, measurements of gloss, surface roughness and static contact angle, and peeling test. Mineralogical changes were determined by x-ray diffraction and molecular changes by Fourier transform infrared spectroscopy. Moreover, micromorphological and chemical characterization of the surfaces was conducted by scanning electron microscopy.

Physical-mechanical changes, such as craquelure and paint loss, depended on the texture of the granite. More specifically, paint on the granite with the finest grain size showed most intense cracking and loss of material. Chemical changes, which were not related to the granite substrate, were most intense in the red and silver paint coatings. In the red paint, loss of binder was accompanied by an intense fading of the colour (due to titanium dioxide relative enrichment), while in the silver paint coating, chemical changes occurred in both the organic binder and aluminium particles, thus darkening the colour. Fewer chemical changes were observed in the blue and black paints. Physical and chemical changes detected in these paints were not correlated.

* Corresponding author.
E-mail address: ipozo@uvigo.es (J.S. Pozo-Antonio).

http://dx.doi.org/10.1016/j.scitotenv.2022.154169

1. Introduction

Since the beginning of the 2000s, contemporaneous mural paintings have become part of the public space in city centres worldwide as a consequence of municipal initiatives through contests and festivals or campaigns to beautify degraded urban areas. Like any paintwork exposed to the environment, and as a consequence of the fact that most of them were not applied on a preparation layer, most of these murals have begun to show signs of deterioration, including loss of cohesion, loss of material, chromatic alterations, fading and biological colonization. Deterioration of contemporaneous mural paintings is occurring at a much higher rate than in other types of cultural property, which can possibly be attributed to 1) the more aggressive atmosphere of the urban space; 2) the convergence of multiple deterioration factors, including anthropogenic factors, owing to the complexity of urban environments, and 3) the lower resistance of modern paints than of ancient paints to the environment, especially to sunlight.

Graffiti spray paints are among the most common types of paint used in contemporary murals, as they easy to apply and their versatility allows artists to produce different textures and finishes. Graffiti spray paints are also used in acts of vandalism. Indeed, the first studies in the field of cultural heritage conservation characterizing graffiti spray paints focused on removal methods (Rivas et al., 2012; Sanmartín et al., 2014; Pozo-Antonio et al., 2016; Gomes et al., 2017). Graffiti spray paints are composed of a pigment (organic or inorganic), an organic binder, a solvent, extenders or fillers and additives (Christie, 2001; Marrion, 2004). Organic pigments (e.g. azo, phthalocyanine and quinacridones) generally produce more intense and brighter colors than inorganic pigments. Graffiti paints usually contain acrylic, alkyd or polyvinyl acetate resins as binders and a solvent that allows the pigment/binder mixture to flow (e.g. water, hexane, cyclohexane, white spirit). Extenders or fillers are white or colourless powders that are very poorly soluble in water and preferably inert to the action of acids and alkalis, and they are used as opacifier, to control flow, to improve the strength of the film and to reduce the sheen. The extenders most commonly used include titanium dioxide (TiO_2), calcite ($CaCO_3$), magnesium carbonate ($MgCO_3$), talc ($Mg_3Si_4O_{10}(OH)_2$), barite ($BaSO_4$), wollastonite ($CaSiO_3$) and fumed silica. Finally, additives with various functions are used to adjust different compositions: coalescing agents, defoamers, freeze–thaw agents, pH buffers, biocides, thickeners and wetting and dispersing agents (Christie, 2001; Marrion, 2004).

Regarding the forms of alteration detected on public artworks, some research on contemporary murals can be found (La Nasa et al., 2016, 2021; Bosi et al., 2020). However, many research studies have addressed the resistance of this type of paint, mainly based on alkyd or acrylic binders, to the main weathering agent that affects modern paintings, i.e. light radiation (Whitmore and Colaluca, 1995; Melo et al., 1999; Chiantore et al., 2000; Chiantore and Lazzari, 2001; Allen et al., 2002, 2018; Learner et al., 2002; Scalarone et al., 2005; Doménech-Carbó et al., 2011; Pintus et al., 2016; Sanmartín and Pozo-Antonio, 2020). In these studies, which form part of the fundamental research on organic polymers, the paints (generally applied to glass) were usually irradiated (with artificial sunlight, UV −A, B or C radiation) and the molecular and/or chemical changes produced in the organic components of the paints (both the binder and the pigment) and that explain the loss of colour were determined. Light radiation in the presence of oxygen induces photo-oxidation, which appears to be the main pathway of deterioration in paints, mainly via scission and cross-linking reactions that produce a series of reactive intermediates and radicals (Whitmore and Colaluca, 1995; Melo et al., 1999; Chiantore et al., 2000; Pintus et al., 2016). In acrylic paints, chain scissions tend to prevail over cross-linking reactions when short alkyl side groups such as methyl or ethyl groups, are involved, accompanied by macromolecular coupling reactions (Whitmore and Colaluca, 1995; Chiantore et al., 2000; Chiantore and Lazzari, 2001). In alkyd paints, the effect of photo-oxidation is similar to that observed in oil paints, causing the following: autoxidation due to the presence of natural antioxidants followed by polymerization and intense cross-linking producing a very stiff, brittle material; chain scission with prevalent β-scission; loss of volatile products such as aldehydes, alcohols and carboxylic acids; fading; and yellowing (Saunders, 1973; Ploeger et al., 2008, 2009). Learner et al. (2002) and Pintus et al. (2016) reported that acrylic paints are more resistant to yellowing than alkyd paints. Pintus et al. (2016) exposed acrylic and alkyd paints to artificial sunlight (wavelengths between 295 and 3000 nm) and found that photo-oxidation of the acrylic paints led to production of oligomers, and the alkyd samples were mainly characterized by a decrease in unsaturated fatty acids.

Different chemical and physical changes have been reported in relation to the light source used. UV-B radiation caused physical (discoloration) and chemical changes in coloured alkyd graffiti paints, and UV-A and daylight were considered less harmful (Sanmartín and Pozo-Antonio, 2020). Whitmore and Colaluca (1995) exposed acrylic dispersions on glass plates to natural ageing in darkness and subsequently to accelerated thermal and UV radiation exposure tests, observing that in darkness, the films acquired a haze and slight yellow discoloration due to weak crosslinking, within a few weeks. The paintings exposed to UV light showed a slight loss of tensile strength and an increase in solubility, suggesting breakdown by chain scission reactions. The weak changes that occurred in the paintwork under UV radiation revealed a high level of resistance to photochemical degradation. Doménech-Carbó et al. (2011) subjected acrylic paintwork to solar irradiation by xenon arc lamps and found that after 800 h, the chroma had decreased considerably and lightness had increased substantially. Likewise, it was confirmed that paints containing inorganic pigments display fewer chroma variations than paints containing organic pigments. Moreover, the presence of inorganic pigments or extender or fillers, such as titanium dioxide, may have either a protective effect by absorbing and/or screening the UV light or they may be photo-active and catalyse photo-degradation of the organic resin (Allen et al., 2002, 2018).

Although paints with other binders such as polyethylene should be more resistant than those with alkyd or acrylic ones due to the absence of unsaturated double bonds in their backbone (Gewert et al., 2015), the heterogeneous composition of the paints (binder, pigment, solvent, extenders and additives) makes necessary to carry out research focused on the behaviour of these paints under different environments, such as natural outdoor exposition or specific radiation lights.

All of the cited studies above evaluated the resistance of different paints to light irradiation under controlled laboratory conditions, as required to determine the effects of particular weathering agents. However, in order to be able to predict the changes that will take place under particular environmental and site conditions, the most suitable method is to expose the material to the specific natural environment. Results obtained by means of this approach are of great interest in the field of heritage conservation, and specifically, for artists or commissioners who, in order to make the artworks more durable, can select the paints that will be most resistant in the specific environment considered.

In studies testing the durability of paints under controlled conditions, the influence of the type of support on paint durability is not generally taken into account. The support can influence the drying process and also polymerization (favouring the appearance of failure features) in freshly applied and dried paint. Therefore, the support may determine adhesion of the paint, polymerization and drying processes, due to for example a pH incompatible with the optimal pH for coating polymerization (e.g. concrete). The support may also influence the durability of the dry paint depending on its thermal inertia or its coefficient of expansion due to temperature or humidity oscillations. Moreover, the porosity of the support may facilitate the action of deterioration factors such as saline solutions. Therefore, in urban pictorial art, which uses a myriad of supports (concrete, steel, glass, wood, rock, brick, etc.), the support-painting interaction will be of great importance regarding the deterioration expected.

In this study, the durability of three non-metallic (red, blue and black) alkyd graffiti spray paints and one metallic (silver) polyethylene graffiti spray paint applied to two types of granites differing in texture and composition was evaluated after exposure to a real outdoor environment. Paint-granite mock-ups were exposed during ten years to a natural urban-marine environment near Vigo (NW Spain), one of the most populated cities on the Atlantic coast of Iberian Peninsula (Vigo, NW Spain). The work

sought to determine the influence of the graffiti spray paint composition and the interaction between the paint and type of granite on the paint durability, by analysing the compositional and textural modifications that had occurred during ten years of exposure.

2. Materials and methods

2.1. Supports

Two types of granite with different texture and mineralogy were selected for study: Rosa Porriño and Vilachán. Rosa Porriño is an ornamental granite (Fig. 1A) that is commercially exploited in O Porriño (NW Spain): it is a two-mica calc-alkaline coarse-grained granite with a panallotriomorphic heterogranular texture (IGME, 1981a). It is composed of 40% quartz, 27% potassium (K) feldspar (orthose), 14% plagioclase, 8% biotite, 2% muscovite and 9% accessory minerals. The main physical characteristics of Rosa Porriño are very low open porosity (0.84%, obtained following UNE-EN 1936:2007) and a pinkish hue of K-feldspar grains.

Vilachán is a fine-grained panallotriomorphic heterogranular adamellite (IGME, 1981b) that is commercially exploited in Tomiño (NW Spain) and used in the architectural and archaeological heritage in the area (Fig. 1B). Vilachán granite is composed of 47% quartz, 18% muscovite, 15% plagioclase, 10% K-feldspar, 7% biotite and 3% accessory minerals. It has an open porosity (UNE-EN 1936:2007) of 2.82% and has yellowish brown bands (i.e. flow textures) typical of the NW peninsula granites that have undergone the last two phases of the Hercynian origin (Escuder et al., 2001; Rivas et al., 2020).

Twenty-four samples of both types of granite, with a disc cutting-finish and of dimensions 3 cm × 10 cm × 2 cm, were cut for application of graffiti spray paint.

2.2. Graffiti spray paints

Four previously characterized graffiti spray paints (Rivas et al., 2012) were acquired from Montana Colors Mtn® (https://www.montanacolors.com/): ultramarine blue (R-5002), devil red (R-3027), graphite black (R-9011) and silver chrome.

As reported by Rivas et al. (2012), the blue, red and black graffiti spray paints were composed of alkyd and polyester resins, while the silver graffiti spray paint was a polyethylene-type polymer.

Each graffiti spray paint was applied to 6 samples (3cmx10cmx2 cm) of each granite, following the same procedure reported by Rivas et al. (2012). Briefly, each paint was sprayed onto the stone surface, from a distance of 30 cm, for 3 s, at an angle of 45□. The painted samples (in total, 48) were held under laboratory conditions (18 ± 5 °C and 60 ± 10% RH) for one month, and 3 of each the 6 replicate samples were exposed to a natural outdoor environment during 10 years (until 2020), and the other 3 samples were kept in the laboratory as control samples. The exposed samples were given codes that refer to the stone to which they were applied (R-Rosa Porriño; V-Vilachán), followed by the paint colour code (R-red; BU-blue; B-black; S-silver); the reference (control) samples were identified by the subscript $_{ref}$.

2.3. Natural exposure

The samples were placed at an angle of 60° on a windowsill between 31 January 2010 and 31 January 2020 (10 years) on the southwest façade of the Mining and Energy Engineering School (42°10´8”N, 8°41´22”W) in the University of Vigo campus (Vigo, Spain, Fig. 1C, D). The campus is located at 10 km from Vigo city centre, at 495 m above sea level and 8.2 km from the Atlantic sea coast. The windowsill where the samples were placed faces the sea (S45°W) (Fig. 1C, D). Vigo (population 300,000) is a major Atlantic port city in terms of industrial, commercial,

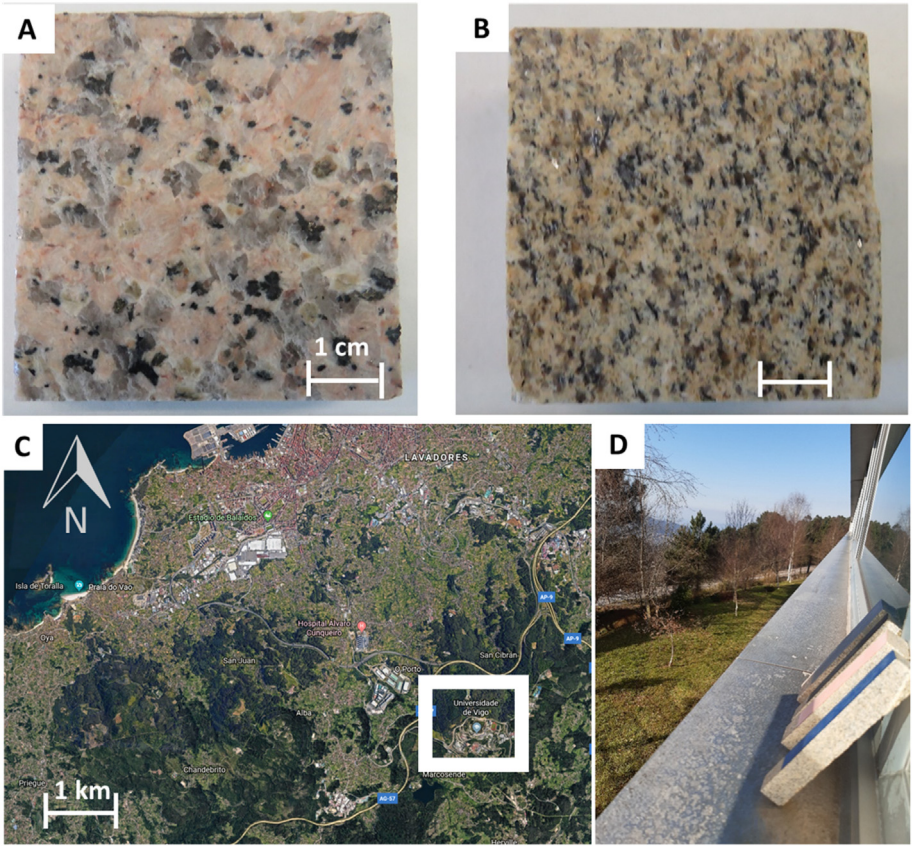

Fig. 1. A) Rosa Porriño granite; B) Vilachán granite; C) Location of the Mining and Energy Engineering School (42°10´8”N, 8°41´22”W, 495 msl), University of Vigo (Vigo, Spain). D) Samples placed on the windowsills of the Mining and Energy Engineering School.

fishing and shipbuilding activities. Following the FAO's agroecological zoning system, the area corresponds to a humid subtropical climate characterized by rainy winters (1800 mm rainfall) (Martínez-Cortizas, 1987; Martínez-Cortizas and Pérez, 1999), an average annual temperature of 15 °C and a strong influence of humid low-pressure S–SW fronts from the Atlantic Ocean. Following the Köppen–Geiger climate classification system, the location has a Cfb type-oceanic climate (Kottek et al., 2006). For more specific characterization of the exposure site, data on climatic parameters (temperature, humidity, precipitation, insolation and wind) and air quality were collected from the network of meteorological stations of the regional government (Xunta de Galicia, accessed 28 September 2020). The monthly mean, mean of the monthly maximum and mean of the monthly minimum air temperature values for the 10-year study period are shown in Table 1. The relative humidity, sunshine hours, relative insolation, irradiation and wind speed and direction were recorded at the weather station on the university campus. The monthly mean concentrations of SO_2, NOx and particulate matter (PM10 and PM2.5), recorded at an air quality data station located in Vigo city centre, were obtained, and the mean values for the period 2010–2019 were calculated. Finally, information on the composition of the wet deposition was collected, although this information is only available for four years (2010 − 2013) during the exposure period.

The temperate humid character of the climate in the area of exposure was confirmed: average temperature of 13.4 °C and a low seasonal thermal oscillation (average of the minimum temperature values of 8.2 °C and average of the maximum values of 19 °C) (Table 1). The temperate character was also indicated by the small number of days (204 days) with frost during the 10 years. Relative humidity was high: the mean value of the minimum did not fall below 62.4%. Calculation of the monthly average accumulated rainfall for the 10 years assumed an annual precipitation of 1142 mm per year, which is slightly lower than the value for the reference series (1981–2010) in Galicia, which is 1229 mm per year (Xunta de Galicia, accessed 28 September 2020). The prevailing wind direction (211°) coincides with the orientation of the façade (S45°W - 215°) where the samples were exposed and with the direction of entry of rainy fronts, which enter from the southwest, from the Atlantic Ocean. The monthly mean concentrations of SO_2, NOx and particulate matter, recorded at a weather station located in the centre of the city of Vigo (NW of the campus), were considered low (as they did not exceed any regulatory limits during the 10 years), and the impact of these pollutants was therefore also expected to be low, taking into account the prevailing wind direction and the dense arboreal and shrub vegetation surrounding the campus (relative to the sparse vegetation in the surroundings of the exposure site). Finally, the marine influence strongly affected the composition of the rain, as indicated by the monthly average concentration of ions in the wet deposition, with Cl^- and Na^+ ions present in the highest concentrations. However, although the SO_4^{2-} content was not among the highest in cities in Galicia, it may be relevant as a source of sulphates in architectural surfaces, as shown in a previous study on the influence of the composition of the aerosol in the conservation of granite facades in the same geographical area (Rivas et al., 2014).

Table 1
Environmental data corresponding to the exposure site. The 10 year averages (2010 − 2019, $n = 10$) were calculated from the average monthly temperature (°C), accumulated rainfall (mm), relative humidity (%), relative insolation (%), irradiation (10 kJ/m^2.year), sunshine hours and speed (km/h) and wind direction (°) recorded at the University of Vigo campus meteorological station; 10 year averages were also calculated for maximum and minimum monthly average temperature, accumulated rainfall and relative humidity (in brackets). The 9 year averages ($n = 9$) were calculated from the annual averages of SO_2, NO_x, PM10 and PM2.5 (μg/m^3) recorded in Vigo city centre (100 msl), and the 4 year averages (2010–2013) were calculated from monthly average ion content (μeq/L) of the wet deposition recorded at the same air quality stations.

Average (max – min) monthly temperature	13.48 (8.2–19)
Number of days with frost (for 10 years)	204.00
Average (max-min) monthly accumulated rainfall	95.17 (2–355)
Average (max-min) monthly relative humidity	82.53 (95.6–62.4)
Hours of sunshine per month	173.4
Monthly relative insolation (%)	46.2
Monthly global irradiation	1318.4
Monthly average of wind speed	7.4
Monthly average of preferential wind direction	211.8
Monthly average of SO_2 (μg/m^3)	3.3
Monthly average of NO_x (μg/m^3)	23.3
Monthly average of PM10 (μg/m^3)	23.5
Monthly average of PM2.5 (μg/m^3)	23.6

Monthly mean values of wet deposition (μeq/L) (mean for 4 years 2010–2013)

Cl^-	NO_3^{2-}	SO_4^{2-}	Na^+	NH_4^+	K^+	Mg^{2+}	Ca^{2+}
292.5	41.8	64.7	180.7	56.3	78.0	49.4	66.3

2.4. Analytical techniques

The following analytical techniques were applied to exposed and control samples, to evaluate the physical and chemical changes at the end of the exposure period:

- The surfaces were examined by stereomicroscopy (SMZ800 Nikon).
- The colour of the exposed and control samples was characterized using CIELAB and CIELCH colour spaces (CIE S014-4/E:2007), with a Minolta CM-700d spectrophotometer. In the CIELAB space, L* (lightness), a* and b* (colour coordinates) were measured. L* represents lightness, ranging from 0 (absolute black) to 100 (absolute white); a* indicates the colour position between red (positive values) and green (negative values) and b* between yellow (positive values) and blue (negative values). In the CIELCH colour space, L* also represents lightness, C* represents the chroma or colour saturation, corresponding to $C^* = [(a^*)^2 + (b^*)^2]^{1/2}$ and h_{ab} represents the hue, calculated as $h_{ab} = \tan [1 - (a^*/b^*)]$. Twenty measurements were made at random on each sample to produce statistically consistent results; each measurement was the average of three ($n = 180$ for condition-stone and paint-). The measurements were made in the Specular Component Excluded (SCE) mode, for a spot diameter of 8 mm, with D65 as illuminant and an observer angle of 10°. Colorimetric differences were processed as colour differences (ΔL^*, Δa^*, Δb^*, ΔC^*_{ab} and ΔH^*) and global colour change (ΔE^*_{ab}) considering the colour of the control samples as the reference (CIE S014-4/E:2007). Therefore, higher values indicate the most visible colour changes.
- The gloss value (G) of the control and the exposed surfaces was measured and the change (ΔG), considering the gloss value of control samples as the reference, was determined using a Konica Minolta Unigloss 60Plus, with a reflection angle of 60°. Three measurements were made per sample ($n = 9$ for condition).
- The surface roughness of the exposed and control samples was measured with a profilometer (Mitutoyo SJ400), following UNE-EN ISO 4288:1999. The parameters measured were the arithmetic average roughness (Ra, μm) and the average maximum profile height (Rz, μm). For each granite sample, the equipment traced three scans of length 2 cm ($n = 9$ for condition).
- The static contact of surfaces of the exposed and control samples was determined using a goniometer (SEO Phoenix-300 Touch), following standard BS EN 828:2013. The sessile drop method (each drop contained 6 μL of deionized water per sample) was applied (n = 9 for condition).
- In order to study the level of adhesion of the paint to the stone, a peeling test (Drdácky et al., 2012) was conducted on the surfaces of the exposed and control samples, using double-sided adhesive tape (TESA Powerbond). Three strips of the adhesive tape (width 10 mm and length 30 mm) were applied to each sample and consecutively removed by pulling at an angle of 90°. The amount of material peeled off was determined as the difference between the weight of the tape after removal from the surface and the weight of the tape before application. The results were expressed as the mean weight of material removed from each surface by the three strips per surface.
- The mineralogical composition of the paint layer in the exposed and control samples was determined by X-ray diffraction (XRD) (with a

Siemens D5000 diffractometer equipped with an X-ray generator: Cu-K_α radiation, Ni filter, 45 kV voltage, and 40 mA intensity). XRD analysis was applied by the powder method. Then, paint powder was collected from the control and aged surfaces by means of an electric grinder. The samples were scanned in 2θ range varying from 1° to 5° with a goniometer speed of 0.05° 2θ s^{-1}.

- The molecular composition of the paint coatings on the exposed and rcontrol samples was determined by Attenuated Transmittance Reflectance–Fourier transform infrared spectroscopy (ATR-FTIR) (Thermo Nicolet 6700 spectrophotometer). Infrared (IR) absorption spectra were recorded at 2 cm^{-1} resolution over 100 scans from 400 to 4000 cm^{-1}.
- Micromorphological and chemical characterization of the surfaces of exposed and control samples was conducted by scanning electron microscopy with energy-dispersive X-ray spectroscopy (SEM-EDS) (Philips XL30) in both Secondary Electron (SE) and Back Scattered Electron (BSE) modes. Optimum observation conditions were obtained at an accelerating potential of 20 kV, a working distance of 9–11 mm and specimen current of 50–60 mA. The acquisition time for recording EDS spectra, i.e. the dwell time, was 40–60 s.

3. Results

Digital photographs of the Rosa Porriño reference samples (on the left of each photograph) and the corresponding exposed samples (right) are shown in Fig. 2. Macroscopically, alterations were observed in all the paints, regardless of the type of granite to which they were applied. All of the paints lost their brightness. Furthermore, intense whitening was observed on the red coating (Fig. 2A), cracking on the blue paint (Fig. 2B) and a whitish film on the blue and black paints (Fig. 2B, C). Loss of brightness was very marked in the silver paint (Fig. 2D). Stereomicroscopic examination of the samples (Fig. 3) confirmed subtle differences in regard to the granite substrate. Thus, the surfaces of the exposed samples of Vilachán coated with the red graffiti spray became rougher than the samples of Rosa Porriño and fissures also appeared in the paint (Fig. 3 A-C). The blue paint on both types of granite displayed intense craquelure (Fig. 3 D- F). On the black paint, craquelure was detected in the Rosa Porriño samples and loss of paint was observed in the Vilachán sample (Fig. 3G-I). Finally, on the silver paint, paint loss was more intense in the Vilachán samples than in the Rosa Porriño samples (Fig. 3J-L.

The ΔE^*_{ab} value was highest in the red paint (Table 2). Different results were obtained for each granite relative to the other paints: in the Rosa Porriño granite, the ΔE^*_{ab} was lowest in the black paint, whereas in the Vilachán granite, the ΔE^*_{ab} was lowest in the silver paint. In all cases, the ΔE^*_{ab} exceeded 3.5 CIELAB units, which is considered the threshold above which the colour change is visible to the naked eye (Mokrzycki and Tatol, 2011).

The colour parameters that contributed to ΔE^*_{ab} were different for each of the paints:

a) In the red paint, the parameters that contributed most to the colour change were L*, which increased, and a*, which decreased. The increase in L* (the highest increase among all the paints) reflected the intense whitening of the surfaces painted in red (Figs. 2 and 3). The difference in a* was also very high, and negative, indicating loss of intensity of the red colour. In general, taking into account the magnitude of ΔC^*_{ab}, the colour of the red painted surfaces of both stones faded (the lightness increased and colour intensity decreased); this effect was quantitatively more intense in the Vilachán granite.
b) In the blue paint, the greatest change occurred in the b* coordinate, which increased. In the Vilachán granite, L* scarcely varied. Therefore, taking into account the magnitude of ΔC^*_{ab}, the qualitative effect of the colour change in this sample was a loss of intensity, i.e. the painted surfaces became greyish in colour. However, in the Rosa Porriño samples, the increase in the b* coordinate was accompanied by a significant increase in L*; hence, in RBU, the colour faded.
c) For the black paint, the ΔE^*_{ab} for both granites was mainly due to an increase in the L*; the magnitude of the change in L* was similar in both granites.
d) Finally, for the silver paint, the ΔE^*_{ab} on both granites was mainly due to a decrease in L*: the coating became darker in colour, particularly those on the Rosa Porriño samples (the decrease was significantly greater in this granite).

The gloss also changed remarkably during the 10-year exposure period (Fig. 4), mainly in blue, black and silver paints. In all of the samples, except RR and VB, the gloss decreased. The greatest ΔG were detected in the blue and the black paints on the Rosa Porriño granite, with decreases greater than 45 GU. The lowest ΔG were detected in the red paint, regardless of the stone. The changes in gloss were greater in the paint on the Rosa Porriño granite samples than on the Vilachán granite samples.

Surface roughness also changed during the exposure (Fig. 5). The changes in Ra (arithmetic average roughness) and Rz (average maximum profile height) followed similar trends. Roughness increased in the blue and black paints and decreased in the silver paint, in a similar way for

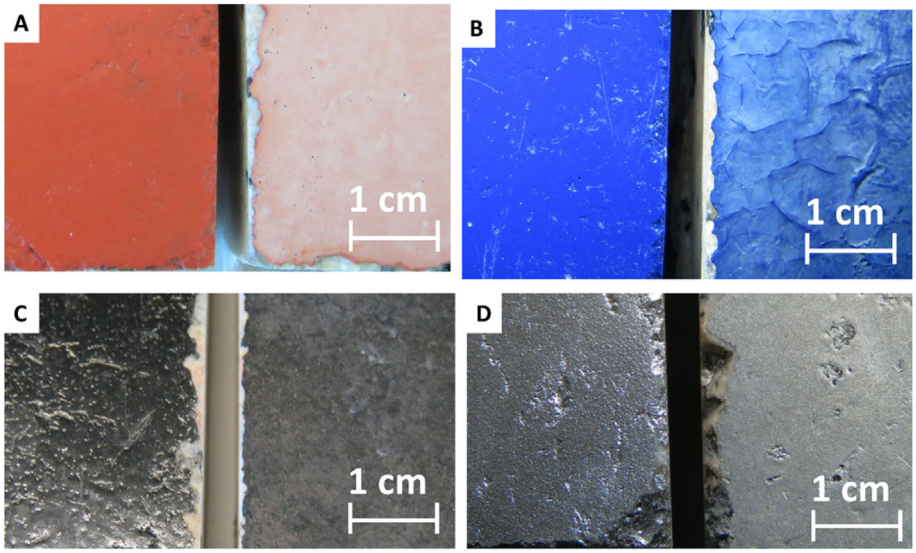

Fig. 2. Macrographs of the surfaces of the reference (left) and exposed (right) samples of Rosa Porriño granite painted with each graffiti spray. A: red paint. B: blue paint. C: black paint. D: silver paint. (For interpretation of the references to colour in this figure legend, the reader is referred to the web version of this article.)

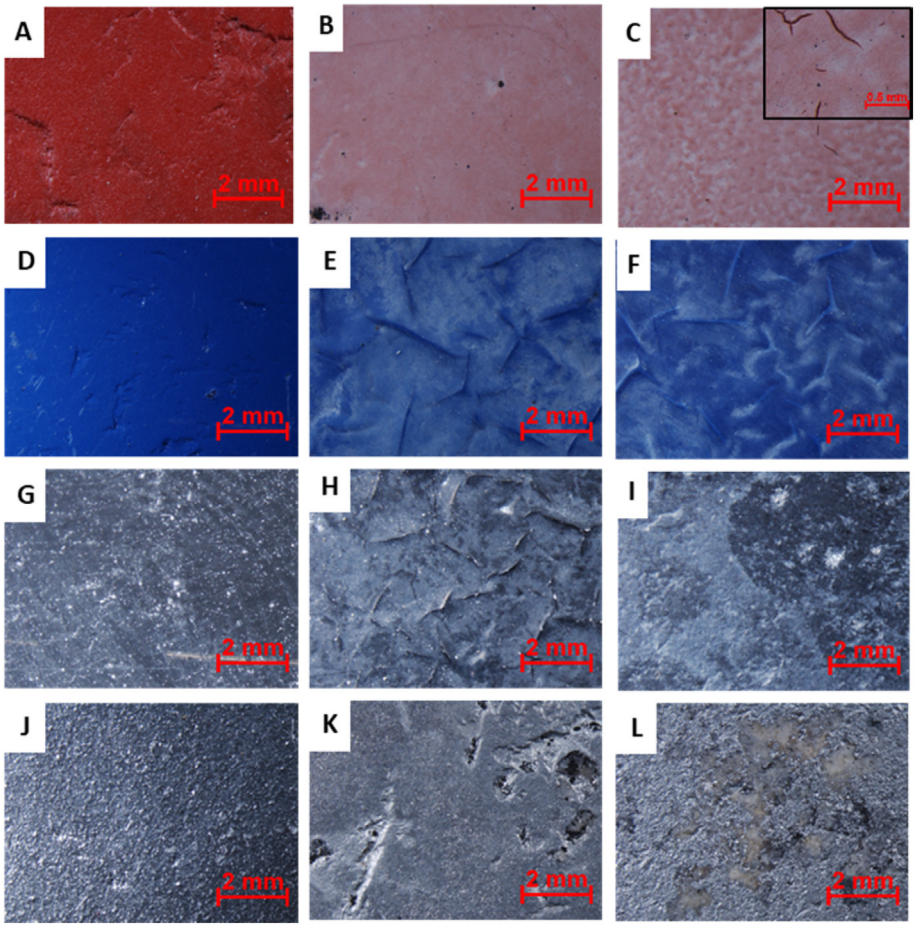

Fig. 3. Stereomicrographs of the reference (column 1, Rosa Porriño) and exposed (column 2 Rosa Porriño and column 3, Vilachán) granite samples. Samples in A, B and C are coated with red paint, samples in D, E and F, with blue paint, samples in G, H and I, with black paint, and samples in J, K, and L, with silver paint. (For interpretation of the references to colour in this figure legend, the reader is referred to the web version of this article.)

Table 2
Colorimetric variation ΔL*, Δa*, Δb*, ΔC^*_{ab} and ΔH* and global colour change (ΔE^*_{ab}) of the exposed samples coated with red (_R), blue (_BU), black (_B) and silver (_S) paint (R_: Rosa Porriño, V_: Vilachán) relative to the colour of the control painted surface.

ID	ΔL*	Δa*	Δb*	ΔC^*_{ab}	ΔH^*_{ab}	ΔE^*_{ab}
ROSA PORRIÑO						
RR	20.57	−22.51	−13.01	−25.97	−1.28	33.15
RBU	14.22	−3.97	18.66	−18.60	−3.99	23.80
RB	11.13	0.09	0.44	−0.44	0.02	11.14
RS	−17.49	0.92	3.90	1.60	−3.68	17.94
VILACHÁN						
VR	23.16	−24.72	−14.39	−28.54	−1.71	36.81
VBU	4.85	−2.57	15.69	−15.73	−2.17	16.62
VB	10.49	−0.03	0.16	0.02	−0.53	10.49
VS	−6.91	0.33	2.45	0.12	−2.46	7.34

both granites. Conversely, different trends were observed in the two type of granite samples coated with red paint: in Vilachán, the roughness increased, whereas in Rosa Porriño, the roughness decreased markedly. Comparison of both types of granite showed that, except for Ra measured on the samples with silver paint (RSD and VSD) and for Rz on samples with black paint (RBD and VBD), greater changes were detected in the Rosa Porriño samples. However, the differences between these samples were not statistically significant.

Fig. 6 shows static contact angles (θ°) of the unpainted Vilachán and Rosa Porriño surfaces, of the control painted samples and the exposed samples. In the painted samples, θ° increased after 10 years of exposure in all cases (with statistically significant differences) (Fig. 6) except in the exposed RR sample (Rosa Porriño with red paint), for which the high standard deviation (±19.3°) precludes determination of statistically significant differences in contact angle. Although this parameter increased, the values never exceeded 90°, which is the threshold above which a surface can be considered hydrophobic (Bico et al., 2002). Values of static contact angles of the unpainted stones were below 90°: 39.2 ± 8.3° for Rosa Porriño and 19.8 ± 11.3° for Vilachán.

Comparison of the results obtained for each granite revealed that in the VR and VBU samples and the respective reference samples (VR_{ref} and VBU_{ref}), the θ° values were higher than in the Rosa Porriño samples, despite the fact that the θ° of the unpainted stones was lower in the Vilachán granite. However, the opposite trend was observed in the samples coated with black and silver paint: in both the reference and the exposed samples, the θ° values were always highest in the Rosa Porriño granite.

The results of the peeling test in the reference and exposed samples are shown in Table 3. In all cases, the weight of material removed by the adhesive tape was considerably lower after the outdoor exposure period, with exception of the silver paint on the Vilachán granite (compare VS with VS_{ref}). In general, the least amount material was removed from the surface coated with blue paint. For the Rosa Porriño granite, the greatest amount of material was removed from the unexposed sample with the red paint coating. For the Vilachán granite, the greatest amount of material was removed from the surface coated with silver paint, regardless of whether the samples were exposed or not exposed.

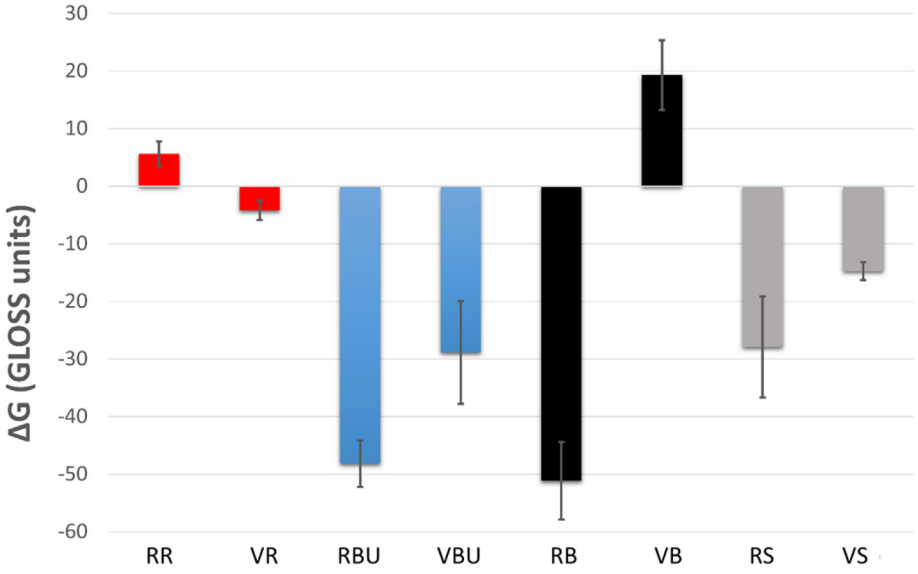

Fig. 4. Changes in gloss (G, gloss units) in the samples after 10 years of exposure relative to the gloss of the control painted surfaces. Values for Rosa Porriño granite (R_) and Vilachán granite (V_) coated with red (_R), blue (_BU), black (_B) and silver (_S) paint are shown. (For interpretation of the references to colour in this figure legend, the reader is referred to the web version of this article.)

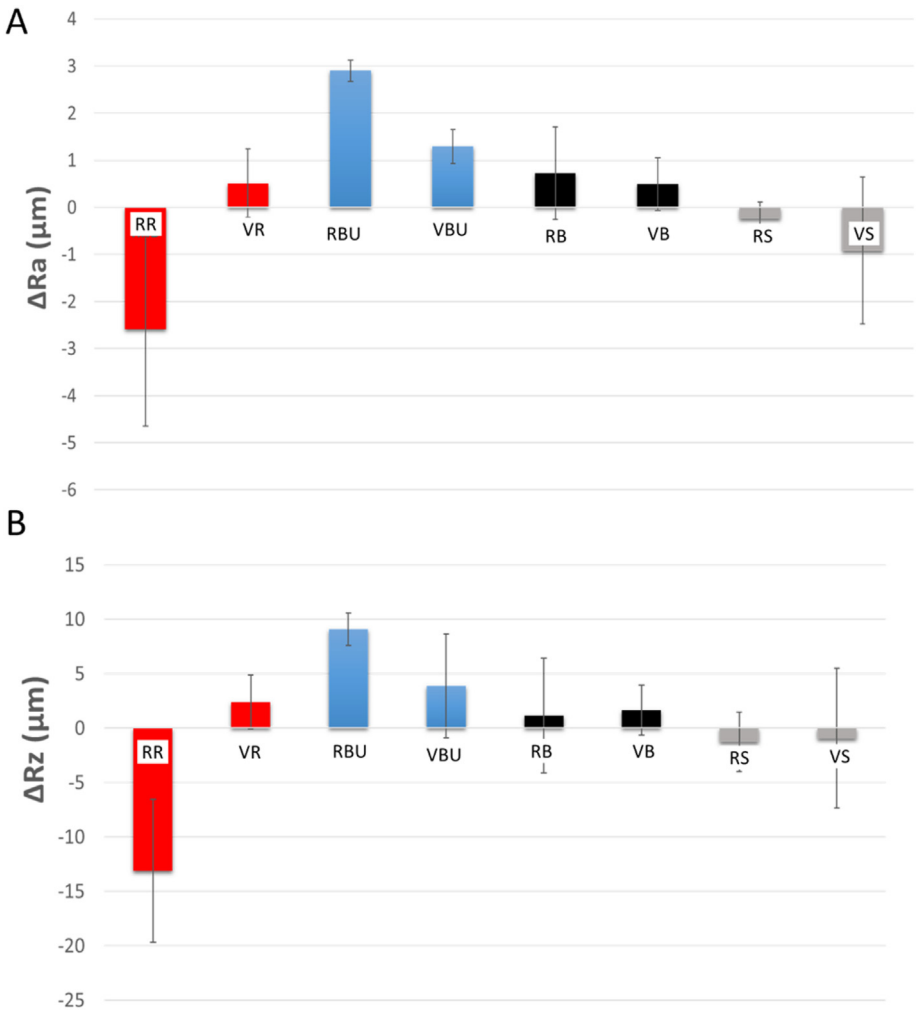

Fig. 5. Changes in roughness parameters (A: Ra, B: Rz, μm) in the samples after outdoor exposure for 10 years relative to the roughness of the control painted surfaces. Values for Rosa Porriño granite (R_) and Vilachán granite (V_) coated with red (_R), blue (_BU), black (_B) and silver (_S) paint are shown. (For interpretation of the references to colour in this figure legend, the reader is referred to the web version of this article.)

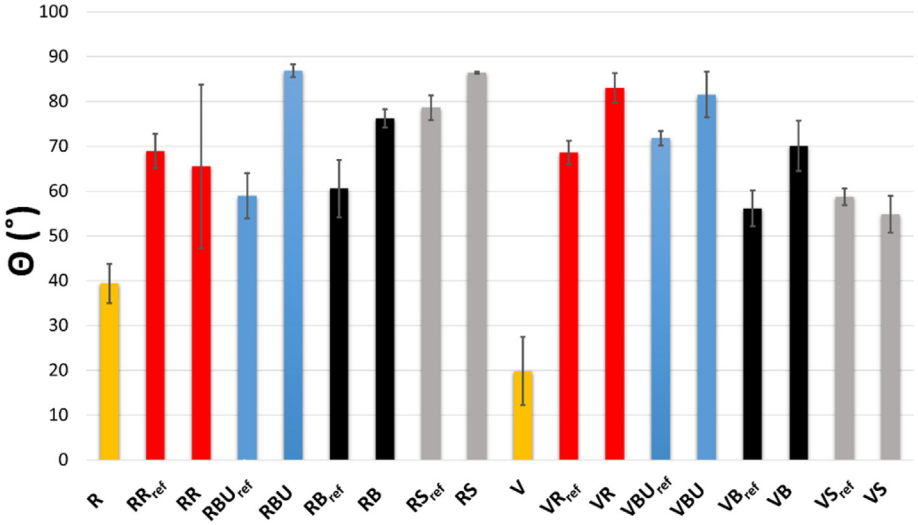

Fig. 6. Static contact angle (θ°) in the unpainted granite samples (R and V) and in the surfaces coated with red (_R), blue (_BU), black (_B) and silver (_S) paint before exposure (_ref in subscript) and after 10 years of outdoor exposure. (For interpretation of the references to colour in this figure legend, the reader is referred to the web version of this article.)

Table 3
Results of the peeling test (mg, average amount of loose matter on three tapes for each sample) in Rosa Porriño (R_) and Vilachán (V_) samples with red (_R), blue (_BU), black (_B) and silver (_S) paints before exposure (_ref in subscript) and after 10 years of exposure. Standard deviations are also shown.

ID	Δm (mg)
RR_{ref}	0.73 ± 0.40
RR	0.27 ± 0.21
RBU_{ref}	0.20 ± 0.10
RBU	0.07 ± 0.12
RB_{ref}	0.40 ± 0.26
RB	0.17 ± 0.21
RS_{ref}	0.50 ± 0.20
RS	0.43 ± 0.06
VR_{ref}	0.53 ± 0.35
VR	0.13 ± 0.12
VBU_{ref}	0.07 ± 0.06
VBU	0.07 ± 0.12
VB_{ref}	0.33 ± 0.21
VB	0.17 ± 0.21
VS_{ref}	0.60 ± 0.40
VS	0.77 ± 0.29

Comparison of the two types of granite showed that, with the exception of the surfaces coated with silver paint, greater amounts of material were removed from the Rosa Porriño samples than from the Vilachán samples.

XRD confirmed that there hasn't been alteration of the inorganic extenders or neoformed mineral phases during the 10-years exposure. In BU, R and S paints on both granites, the same mineral phases present in the unaltered paints were detected in the aged paints (rutile—TiO_2— for the BU, rutile—TiO_2— and barite—$BaSO_4$— for the R and aluminium—Al— for the S) although some of the granite forming minerals were also identified (quartz—SiO_2—, muscovite—$KAl_2(AlSi_3O_{10})(OH)_2$—, albite—$NaAlSi_3O_8$— and biotite—$K(Mg,Fe)_3AlSi_3O_{10}(OH, F)_2$—) whose presence in the samples may be due to their detachment from the stone surface during scraping. In the aged samples of red paint on both granites (RR and VR), graphite—C— was also detected. This mineral, a common extender in paints, could be also present in the unaltered sample in quantities below the detection threshold (ca. 5% wt.) of the XRD equipment. Then, as consequence of the organic phase loss during the 10-years exposure, a relative enrichment of graphite allowed its detection. This mineral was also detected in the aged black paint on Rosa Porriño (RB). It is noteworthy that in black paint in both granites after exposure (RB and VB), rutile—TiO_2— (undetected by XRD in the original paint) has been identified. The detection of this mineral after exposure could be also related to its quantity below the detection threshold as was reported for the graphite.

FTIR spectra of the red, blue and black paint samples (Fig. 7A, B and C respectively) confirmed the alkyd composition of these paints (Socrates, 2001; Rivas et al., 2012; Pintus et al., 2016; Gomes et al., 2018). The FTIR spectrum of the red paint included the following: a sharp band at 3675 cm^{-1} attributed to OH stretching vibration of water; a broad band at around 3600–3300 cm^{-1} corresponding to the OH stretching vibration of water; a faint band at 3077 cm^{-1}, which can be assigned to CH stretching vibrations of aromatic rings; an intense doublet band at 2924 cm^{-1} and 2854 cm^{-1} corresponding to CH asymmetric and symmetric stretching vibrations of methylene groups; intense, sharp bands at 1715 cm^{-1} and 1253 cm^{-1} corresponding to the stretching vibration CO (ester type), weak bands in the range 1624–1481 cm^{-1} assigned to CC aromatic ring; a band at 1452 cm^{-1} assigned to CH bend of CH_3 symmetric deformation; a band at 1363 cm^{-1} assigned to COC; a band at 1116 cm^{-1} assigned to CO stretching phthalic group; bands in the range 1110–1060 cm^{-1} assigned to CO and indicating the presence of esters of unsaturated aliphatic fatty acids and bands in the range 800–700 cm^{-1} assigned to aromatic CH out of plane bending.

The FTIR spectra obtained for the blue (Fig. 7B) and black paint coatings (Fig. 7C) were less complex. For the blue paint, the wide band at 3300–3600 cm^{-1} showed two peaks at 3521 and 3400 cm^{-1} indicating the presence of OH stretching vibration of water. For both paints, the bands assigned to CC in the range 1600–1500 cm^{-1} were absent.

For the silver paint, as reported by Rivas et al. (2012) and Gomes et al. (2018), the FTIR spectrum showed that the functional groups CO, CC and CO are absent and the most intense effects were those for CH asymmetric stretch vibrations of alkanes (Fig. 7D), confirming the predominance of polyethylene-type polymers in this paint. The FTIR spectrum of the silver paint includes absorption bands at 2918 and 2851 cm^{-1} corresponding to CH asymmetric and symmetric stretching vibrations of methylene groups, 1445 cm^{-1} assigned to bending deformation, 1374 cm^{-1} assigned to CH_3 symmetric deformation and 745–700 cm^{-1} corresponding to rocking

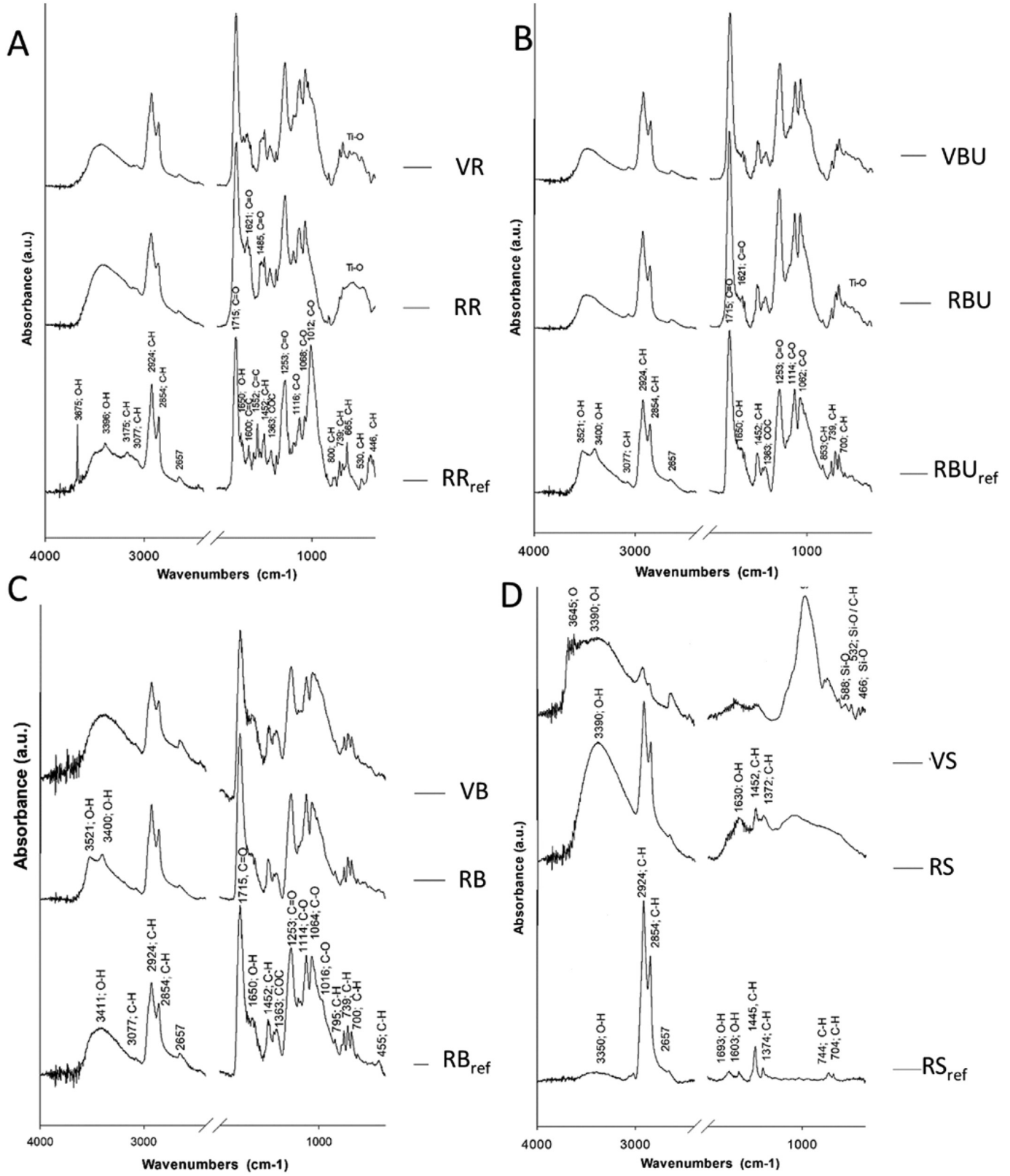

Fig. 7. FTIR spectra of Rosa Porriño (R_) and Vilachán (V_) samples coated with red (_R), blue (_BU), black (_B) and silver (_S) paints after 10 years of outdoor exposure. For comparison with the initial composition, the spectra of reference painted samples of Rosa Porriño granite before exposure (_ref in subscript) are also shown. (For interpretation of the references to colour in this figure legend, the reader is referred to the web version of this article.)

deformation (Gulmine et al., 2002; Rajandas et al., 2012). Weak bands at 3350, 1693 and 1603 cm^{-1} were assigned to OH vibrations as a result of the water/humidity.

After the outdoor exposure period, the most remarkable changes in the FTIR spectra were identified in the silver paint coatings (Fig. 7D). Although the same effects were observed in both types of granite, the greatest

differences were identified in the Vilachán sample (VS, Fig. 7D). It occurred that in the spectra of the aged samples, the bands due to the organic component have decreased, while those due to silicate minerals and water (probably absorbed and adsorbed on the granite forming minerals), such as SiO and OH stretching vibration respectively become dominant. In the FTIR spectra of the Vilachán samples coated with silver paint (VS), several bands below 1000 cm^{-1} were assigned to CH and also to Si-O; the latter assignment confirmed loss of the paint on this granite due to an increase in silicate absorption bands, as detected by stereomicroscopy and XRD.

For the red paint (Fig. 7A) and blue paint (Fig. 7B), regardless of the type of granite, a weak broadening of the band assigned to carbonyl group was detected in the range 1700-1600 cm^{-1} with a peak at 1621 cm^{-1} in the samples with blue paint and in addition, at 1485 cm^{-1} in the samples with red paint. A wide band at 600–450 cm^{-1} was observed in the spectra of the exposed red paint coatings and to a lesser extent in the blue paint coatings, confirming the existence of TiO_2 in the paint composition (Rivas et al., 2012).

In the FTIR spectrum of the black paints after exposure, in the RB sample, two bands at 3521 and 3400 cm^{-1} assigned to OH stretching vibration of water were detected, which were not part of the reference sample.

SEM observations enabled identification of textural and compositional changes in the paints after the exposure period (Figs. 8-11). The composition of the red graffiti paint was based on nanoparticles rich in Si, Mg, Al, Ca, Ti and Fe (Fig. 8A) and that of the blue paint, on Si and Ti (Fig. 9A). These nanoparticles were bound in a C-rich matrix. The black paint was composed of a homogeneous, fine-grained film only containing C (Fig. 10A), and the silver paint was composed by larger aluminium particles than those in the red and blue paints (Fig. 11A). The aluminium particles were dispersed in a C matrix (Fig. 11A).

After the outdoor exposure, the amount of C had decreased considerably in all four paints (compare the C/O ratio from the EDS spectrum of the reference and in the exposed samples). For the exposed red and blue-painted surfaces (Figs. 8B, C and 9 B–D respectively), the EDS spectra showed an increase in Ti relative to the EDS of the reference sample. Moreover, the EDS of the exposed paints showed the presence of Na, Mg, Al, P, S, Cl, K and Zn (Figs. 8B-C, 9B-D). These elements were not identified in the EDS spectra of the reference samples. Moreover, deposits with different morphologies were identified in the different paints:

- In the samples with red paint, voluminous deposits rich in C, Zn, Si, Al and Ti and to a lesser extent Mg, P, S, Cl, K, Ca and Fe were detected (Fig. 8B, C, EDS3,7). Deposits rich in Si, Al, K, Ti and Fe were also detected (Fig. 8B, EDS4).
- In the samples with blue paint, two different deposits were detected on the surfaces: i) cubic deposits rich in Cl, K and Na (Fig. 9C EDS3) and granular deposits composed of Na, Al, Si and to a lesser extent Ti, Mg, P, S, Cl, K, Fe and Zn (Fig. 9C, D EDS4 and 6).
- In the exposed samples with black paint (Fig. 10B, C), agglomerations of particles rich in Al and to a lesser extent Zn were detected (Fig. 10B, EDS2), and small particles rich in Zn, Na, Si, Cl, K, Al, P, S and Ca were also found spread on the surface (Fig. 10C, EDS3, 4).
- The EDS spectra of the exposed samples painted with silver paint indicated the presence of Na, K and Si in the paint (Fig. 11B and C, EDS2, 3 and 5) and granular deposits composed of Al, Si, Zn, Ca, Mg and Fe (Fig. 11B, EDS4). Note that for the Vilachán sample, the aluminium particles seemed to be more compact than in the corresponding reference sample.

4. Discussion

In this research, we investigated how three non-metallic (red, blue and black) alkyd graffiti spray paints and one metallic (silver) polyethylene

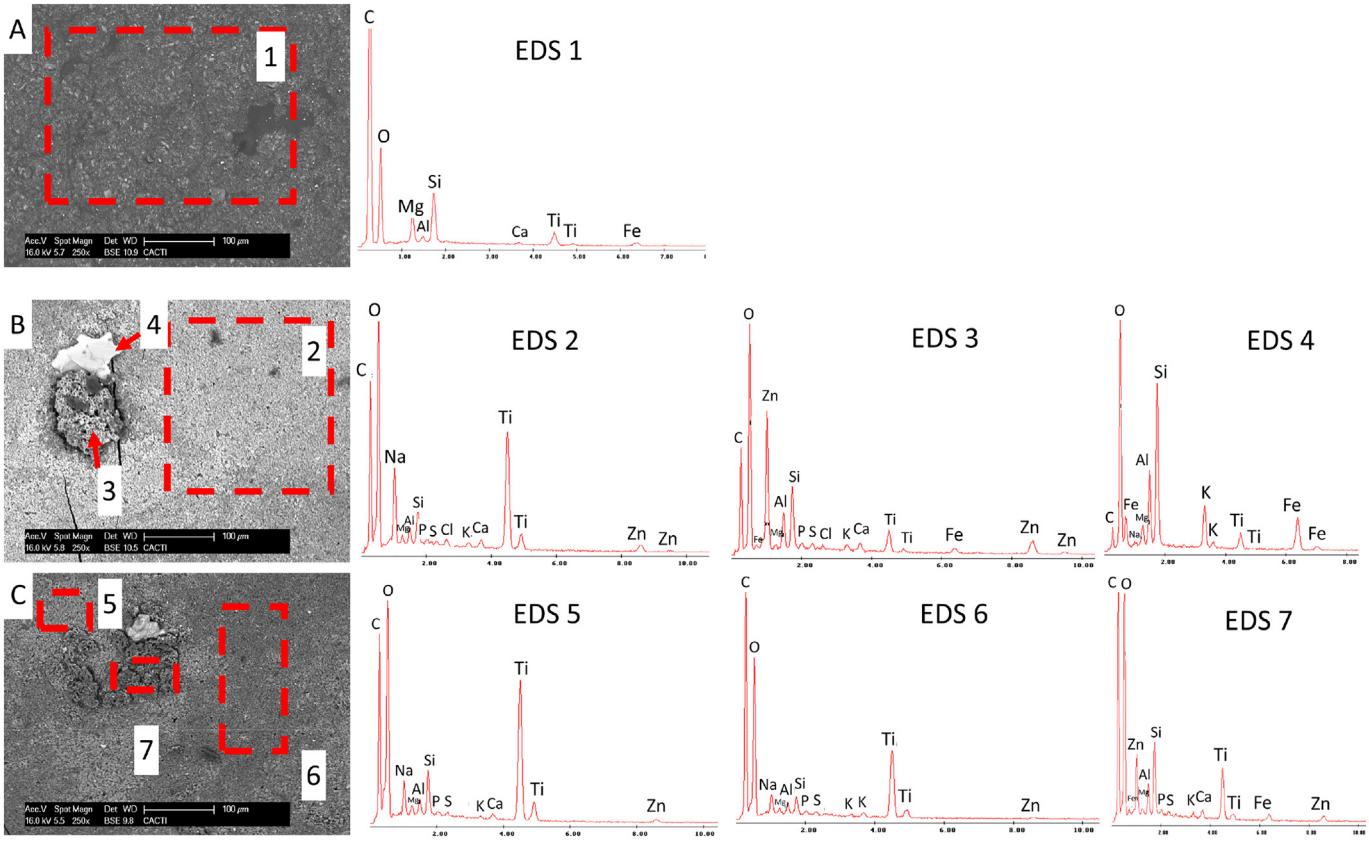

Fig. 8. SEM micrographs and EDS spectra of surfaces coated with red paint. A: Painted reference sample of Rosa Porriño granite. B: Painted sample of Rosa Porriño granite after exposure. C: Painted sample of Vilachán granite after exposure. (For interpretation of the references to colour in this figure legend, the reader is referred to the web version of this article.)

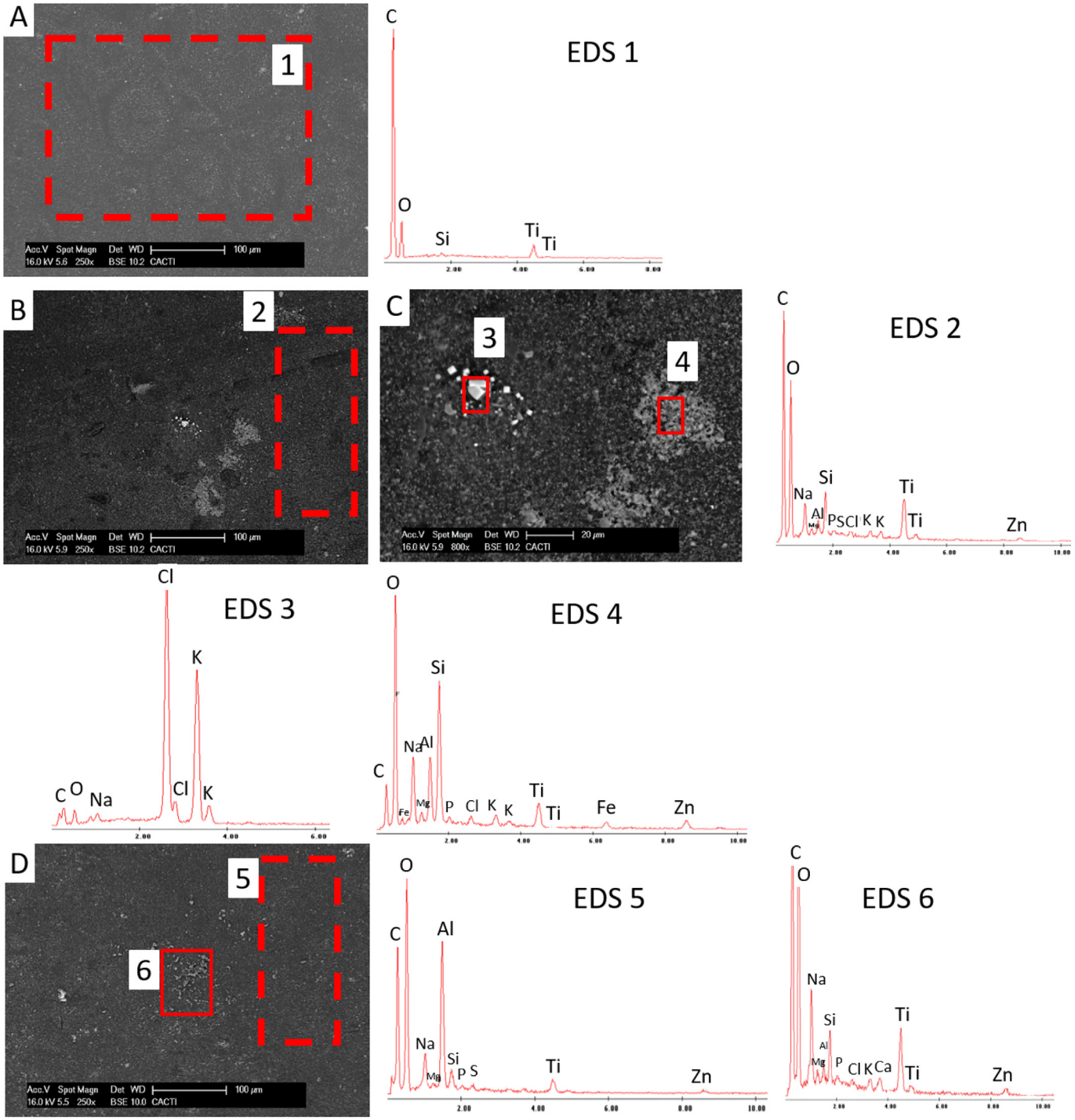

Fig. 9. SEM micrographs and EDS spectra of surfaces coated with blue paint. A: Painted reference sample of Rosa Porriño granite. B-C: Painted sample of Rosa Porriño granite after exposure. D: Painted sample Vilachán granite after exposure. (For interpretation of the references to colour in this figure legend, the reader is referred to the web version of this article.)

graffiti spray paint applied to two types of granite with different mineralogy and texture, i.e. the commercial granites Rosa Porriño and Vilachán, were affected by a decade (2010–2020)-long exposure to a natural urban-marine environment near Vigo (NW Spain). Texture and mineralogy of the granite did not seem to influence on the chemical weathering of the paints but does seem to influence on the physical deterioration: the red, black and silver graffiti paints on the Vilachán granite seemed to undergo more intense weathering than the same paints on Rosa Porriño granite. Indeed, in the Vilachán samples more intense craquelure in the red paint and greater loss of material from the black and silver paints were observed than in the corresponding samples of Rosa Porriño granite. The more intense physical alterations in the Vilachán than in the Rosa Porriño granite may be related to the water movement in the stones through the fissures: the most porous Vilachán granite experienced a more intense water movement through its fissures than the least porous Rosa Porriño granite.

Stereomicroscopic and spectrophotometric analysis showed that the red paint was the paint most strongly affected, followed by the blue paint and then, depending on the underlying granite, either black or silver paints. The lightness of the alkyd (red, blue and black) paints increased, as result of fading (Doménech-Carbó et al., 2011), while the surfaces of the metallic

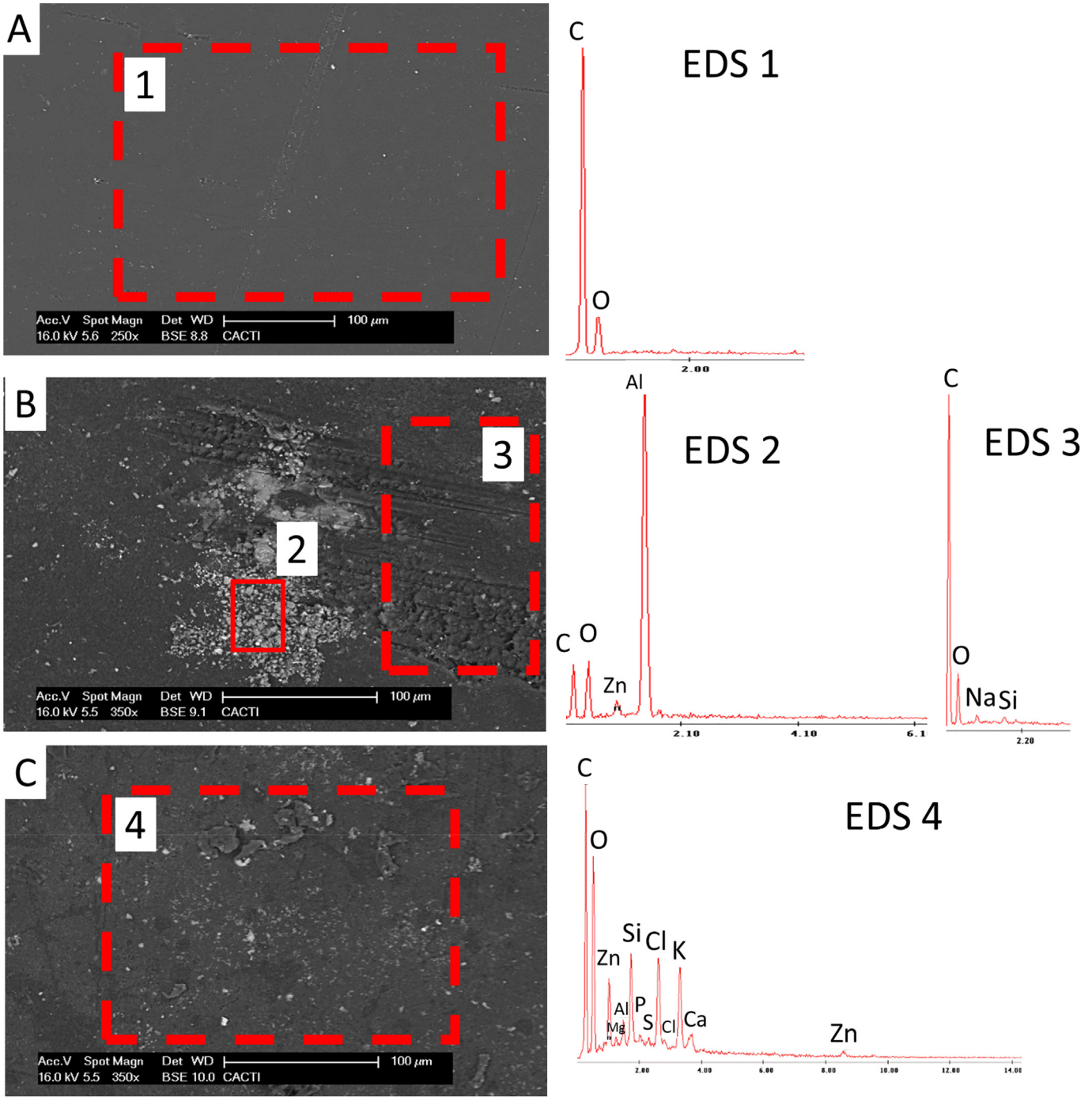

Fig. 10. SEM micrographs and EDS spectra of surfaces coated with black paint. A: Painted reference sample of Rosa Porriño granite. B: Painted sample of Rosa Porriño granite after exposure. C: Painted sample of VIlachán granite after exposure.

silver polyethylene paint became darker (decrease in L*). However, greater variations in gloss were observed in the blue and black graffiti paints: the gloss generally decreased, except in the black paint on the Vilachán. Changes in gloss were least notable in the red paint. Therefore, the colour changes were not related to gloss variations. Roughness was another of the physical properties affected by the outdoor exposure. On the one hand, the increased roughness was related to the craquelure in the paints, mainly in the blue paint. On the other hand, the decrease in roughness of the both granite surfaces coated with the silver paint was related to the intense loss of paint.

The cited darkening detected by spectrophotometry for the silver painted surfaces could be related to: i) modifications of the binder and ii) to chemical changes of the aluminium particles (inorganic pigment). On the one hand, attending to the binder modification, regardless of the underlying granite, silver paint appeared to undergo the greatest chemical modifications, as indicated by the FTIR spectra. The occurrence of the broad band around 3600–3300 cm^{-1} corresponding to the OH stretching vibration, can be assigned to the decomposition of the hydroperoxides formed as primary photoproducts by the scission of the weak OO bond, which gives a macro-alkoxy and a hydroxyl radical OH (Carpentieri et al., 2011; Fotopoulou and Karapanagioti, 2019). This radical can react by several routes: ß-scissions with cleavage of the main chain to form aldehydes, abstraction of hydrogen without cleavage of the chain to form hydroxyls, cage reaction between the pair of the formed radicals giving chain ketones

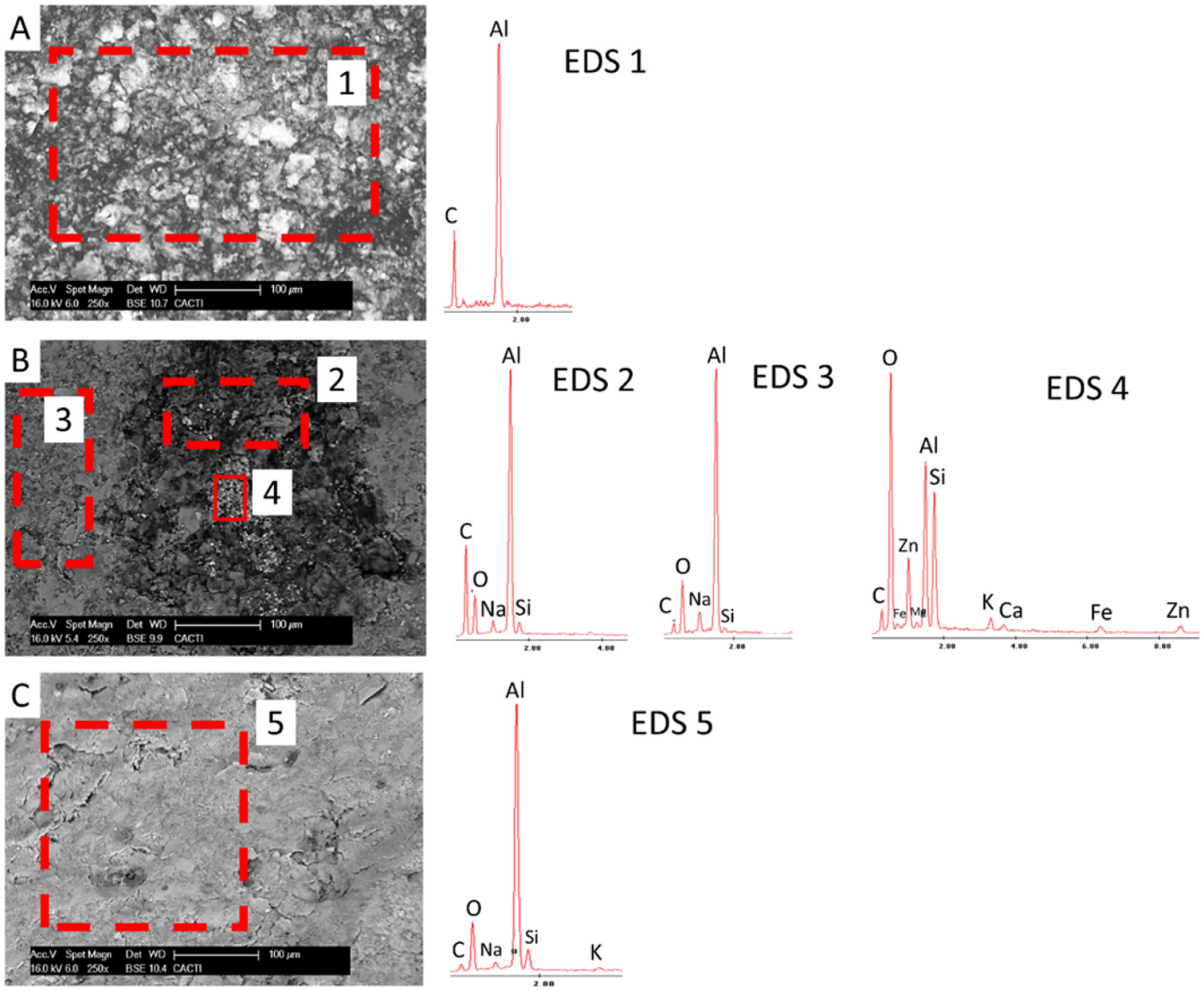

Fig. 11. SEM micrographs and EDS spectra of surfaces coated with silver paint. A: Painted reference sample of Rosa Porriño granite. B: Painted sample of Rosa Porriño granite after exposure. C: Painted sample of Vilachán granite after exposure.

(Carpentieri et al., 2011, Fotopoulou and Karapanagioti, 2019). Ketones photochemically react by Norrish type I or type II reactions (Edge et al., 1991). For polyethylene polymers, the absorption of light is attributed to chromophores added (Fotopoulou and Karapanagioti, 2019). UV irradiation is absorbed by the chromophores which lead to radical formation. As result, free, low molecular weight compounds which can remain in the paint film. As consequence, the material gets brittle and is more susceptible to fragmentation which makes a higher surface area available for further reactions. The low molecular weight compounds increase the hydrophilicity of the polymer (Vasile, 2005; Gewert et al., 2015). However, in this research, although samples were always hydrophilic ($\theta^o < 90^o$, Bico et al., 2002), θ^o increased with exception of the red painted Rosa Porriño and the silver painted Vilachán (both without statistical significant differences in comparison to the control surfaces). These slight θ^o increases can be attributed to the roughness increases (Darmanin and Guittard, 2015; Zhang et al., 2016; López et al., 2019). On the other hand, aluminium particles exposed to environment could undergo chemical changes due to hydroxylation of the oxide film as moisture is absorbed from the air and the colour changes from light to dark (Zahner, 2019). In fact, the intense OH absorption bands in the FTIR spectra of the silver painted samples could not be totally assigned to OH groups in polyethylene binder, because they would be also assigned to the hydroxylation of this oxide film. Marine environments may also induce corrosion of these aluminium particles and subsequent pitting.

Although polyethylene polymers are usually more resistant to photodegradation than alkyd polymers, because the former do not contain any unsaturated double bonds in their polymer backbone and then, they should be immune to photo-initiated degradation (Grassie and Scott, 1988; Gewert et al., 2015), FTIR analysis allowed the identification of more intense chemical changes in the silver polyethylene paint than in the black, red and blue alkyds paints. The inorganic chromophore formed by aluminium particles should be the responsible for photo-initiated degradation (Vasile, 2005; Gewert et al., 2015). In the alkyd paints, the occurrence of bands around 3600–3300 cm^{-1} corresponding to the OH stretching vibration of water is related to the formation of new alcohol groups along the fatty acid portion through either ß-scissions or Norrish type I reactions with the subsequent broadening of the band assigned to carbonyl group in the range 1700–1600 cm^{-1} due to the formation of unsaturated ketones (Lazzari and Chiantore, 1999; Perrin et al., 2000; Pintus et al., 2016).

From the aesthetical point of view, red and blue paints were those with the most affected physical changes during the exposure period (fading for the red paint and craquelure for the blue paint). Therefore, as previously reported (Sanmartín and Pozo-Antonio, 2020), the greater chemical changes

are not related to greater physical changes. The physical changes in these two paints seem to be related to the loss of binder detected by FTIR and SEM. As result of this loss, a relative enrichment in TiO_2 was identified which is correlated to the L* increase.

Regardless of the granite and the paint, SEM analysis enabled identification of granular deposits rich in Si, Al, K, etc., which can be related to the deposition of atmospheric particles on the surfaces. The presence of Cl, K and Na salts is related to the proximity of the sea. Zn was present in the exposed paints in two different formats: i) embedded in the paint and ii) as component of voluminous organic deposits on the surfaces. In the former mode, Zn can become from $ZnSO_4{\cdot}7H_2O$ used to prepare Zn-spiked TiO_2 nanoparticles added during paint manufacturing due to their effective mechanism for photocatalysis (Nguyen et al., 2012). Zn embedded in the paint was found in red, blue and black paints where rutile (TiO_2) was identified by XRD. In the latter, Zn should be exogenous and it would come from the deposition of metalloids and metallic elements such as Cu, Fe, Pb, etc. derived from gasoline and diesel (Santos et al., 2011). Note that samples were located at a distance of 10 m from a busy car parking. Deposits rich in Fe were also detected on the exposed red painted surfaces.

5. Conclusions

Diverse type of weathering effects was observed in graffiti spray paints applied to two types of granite with different texture and mineralogy and exposed to a natural urban-marine environment characterized by wet winters. Three alkyd (red, blue and black) paints and one polyethylene (silver) paint were tested.

Physical and chemical changes in the paints were not correlated. Physico-mechanical changes such as craquelure and paint loss seemed to depend on the water movement through the fissure system. Cracking and paint loss were most intense in the paints applied to granite with the highest porosity: craquelure in the red paint and loss of material in the silver and black paints. Craquelure was associated with increased roughness of the paint surface, while paint loss was associated with decreased roughness. The intense fading of the red paint, regardless of the granite, was attributed to a chemical change associated with loss of binder and the consequent TiO_2 relative enrichment. The chemical changes were not related to the granite substrate; they were most intense in the silver paint and related to the organic binder. These changes of the silver paint could be also associated with darkening of the aluminium particles (inorganic pigment of this paint). Deposits on the surfaces of the four paints resulted from the interaction of the paint with the urban and marine aerosols and road traffic pollutants rich in Na, Cl, K, P, Ca, Mg, Si, Zn and K. The Zn may have originated from petrol fumes, but may also be derived from the $ZnSO_4{\cdot}7H_2O$ used to prepare Zn-spiked TiO_2 nanoparticles added to the paint to improve photocatalysis.

The study findings may be useful for all those professionals dealing not only for the characterization and identification of spray paints, i.e. urban artists who may wish to increase the durability of their wall paintings, but also for analytical chemists, conservation scientists, conservators, restorers, etc. in order to understand their main degradations and for considering conservation decisions.

CRediT authorship contribution statement

J.S. Pozo-Antonio: Conceptualization, Investigation, Resources, Methodology, Software, Data curation, Supervision, Project administration, Writing- Original draft preparation, Writing- Reviewing, Editing and Funding acquisition. T. Rivas: Conceptualization, Investigation, Resources, Methodology, Software; Data curation, Visualization, Supervision, Project administration, Writing- Reviewing, Editing and Funding acquisition. N. González: Investigation, Methodology, Software and Data curation. E.M. Alonso-Villar: Investigation, Methodology, Software and Data curation.

Declaration of competing interest

The authors declare that they have no known competing financial interests or personal relationships that could have appeared to influence the work reported in this paper.

Acknowledgements

This document was produced within the Conservation of Art in Public Spaces (CAPuS) project. The CAPuS project has received funding from the European Commission, Programme Erasmus + Knowledge Alliances 2017 (N°588082-EPP-A-2017-1-IT-EPPKA2-KA). J.S. Pozo-Antonio was supported by the Ministry of Science and Innovation, Government of Spain through grant number RYC2020-028902-I.

References

Allen, N.S., Edge, M., Sandoval, G., Ortega, A., Liauw, C.M., Stratton, J., McIntyre, R.B., 2002. Interrelationship of spectroscopic properties with the thermal and photochemical behaviour of titanium dioxide pigments in metallocene polyethylene and alkyd based paint films: micron versus nanoparticles. Polym. Degrad. Stab. 76, 305. https://doi.org/10.1016/S0141-3910(02)00027-7.

Allen, N.S., McIntyre, R.B., Maltby, J., Hill, C., Edge, M., 2018. Photo-stabilisation and UV blocking efficacy of coated macro and nano-rutile titanium dioxide particles in paints and coatings. J. Polym. Environ. 26, 4243–4257. https://doi.org/10.1007/s10924-018-1298-0.

Bico, J., Thiele, U., Quéré, D., 2002. Wetting of textured surfaces. Colloids Surf. A Physicochem. Eng. Asp. 206, 41–46. https://doi.org/10.1016/S0927-7757(02)00061-4.

Bosi, A., Ciccola, A., Serafini, I., Guiso, M., Ripanti, F., Postorino, P., Curini, R., Bianco, A., 2020. Street art graffiti: discovering their composition and alteration by FTIR and micro-Raman spectroscopy. Spectrochim. Acta A Mol. Biomol. Spectrosc. 225, 117474. https://doi.org/10.1016/j.saa.2019.117474.

BS EN 828:2013, 2013. Adhesives. Wettability. Determination by Measurement of Contact Angle and Surface Free Energy of Solid Surface.

Carpentieri, I., Brunella, V., Bracco, P., Paganini, M.C., Del Prever, E.M.B., Luda, M.P., Bonomi, S., Costa, L., 2011. Post irradiation oxidation of different polyethylenes. Polym. Degrad. Stab. 96, 624–629.

Chiantore, O., Lazzari, M., 2001. Photo-oxidative stability of paraloid acrylic protective polymers. Polymer 42, 17–27. https://doi.org/10.1016/S0032-3861(00)00327-X.

Chiantore, O., Trossarelli, L., Lazzari, M., 2000. Photooxidative degradation of acrylic and methacrylic polymers. Polymer 41, 1657–1668. https://doi.org/10.1016/S0032-3861(99)00349-3.

Christie, R.M., 2001. Colour Chemistry ISBN 0-85404-573-2. 215p.

CIE S014-4/E:2007, 2007. Colorimetry Part 4: CIE 1976 L*a*b* Colour Space, Commission Internationale de l'eclairage, CIE Central Bureau, Vienna.

Darmanin, T., Guittard, F., 2015. Superhydrophobic and superoleophobic properties in nature. Mater. Today 18, 273–285.

Doménech-Carbó, M.T., Silva, M.F., Aura-Castro, E., Fuster-López, L., Kröner, S., Martínez-Bazán, M.L., Más-Barberá, X., Meeklenburg, M.F., Osete-Cortina, L., Doménech, A., Gimeno-Adelantado, J.V., Yusá-Marco, D.J., 2011. Study of behavior on simulated daylight ageing of artists' acrylic and poly(vinyl acetate) paint films. Anal. Chem. Cult. Herit. 399 (9), 2921–2937. https://doi.org/10.1007/s00216-010-4294-3.

Drdácky, M., Lesák, J., Rescie, S., Slízková, Z., Tiano, P., Valach, J., 2012. Standardization of peeling test for assessing the cohesion and consolidation characteristics of historic stone surfaces. Mater. Struct. 45, 505–520. https://doi.org/10.1617/s11527-011-9778-x.

Edge, M., Hayes, M., Mohammadian, M., Allen, S.N., Jewitt, S.T., 1991. Aspects of poly(ethylene terephthalate) degradation on archival life and environmental degradation. Polym. Degrad. Stab. 32, 131–153.

Escuder, J., Carbonell, R., Martí, D., Pérez-Estaún, A., 2001. Interacción fluido-roca a lo largo de las superficies de fractura: efectos mineralógicos y texturales de las alteraciones observadas en el Plutón Granítico de Albalá, SO del macizo Hercínico Ibérico. Bol. Geol. Min. 112 (3), 59–78.

Fotopoulou, K.N., Karapanagioti, H.K., 2019. Degradation of various plastics in the environment. Handbook of Environmental Chemistry. 78, pp. 71–92.

Gewert, B., Plassmann, M.M., Macleod, M., 2015. Pathways for degradation of plastic polymers floating in the marine environment. Environ Sci Process Impacts 17 (9), 1513–1521.

Gomes, V., Dionísio, A., Pozo-Antonio, J.S., 2017. Conservation strategies against graffiti vandalism on cultural heritage stones: protective coatings and cleaning methods. Prog. Org. Coat. 113C, 90–109. https://doi.org/10.1016/j.porgcoat.2017.08.010.

Gomes, V., Dionísio, A., Pozo-Antonio, J.S., 2018. The influence of the SO2 aging on the graffiti cleaning effectiveness with chemical procedures on a granite substrate. Sci. Total Environ. 625, 233–245. https://doi.org/10.1016/j.scitotenv.2017.12.291.

Grassie, N., Scott, G., 1988. Polymer Degradation & Stabilisation. 1988. Cambridge University Press, Cambridge England, New York.

Gulmine, J.V., Janissek, P.R., Heise, H.M., Akcelrud, L., 2002. Polyethylene characterization by FTIR. Polym. Test. 21 (5), 557–563.

IGME, 1981a. Mapa Geológico de España E 1:50.000, 261 sheet-Tui, Segunda Edición, Servicio de Publicaciones, Ministerio de Industria y Energía.

Igme, 1981b. Mapa Geológico de España E 1:50.000, 223 sheet-Vigo, segunda Edición, servicio de publicaciones, ministerio de industria y Energía.

Kottek, M., Grieser, J., Beck, C., Rudolf, B., Rubel, F., 2006. World map of the Köppen-Geiger climate classification updated. Meteorol. Z. 15, 259–263. https://doi.org/10.1127/0941-2948/2006/0130.

La Nasa, J., Orsini, S., Degano, I., Rava, A., Modugno, F., Colombini, M.P., 2016. A chemical study of organic materials in three murals by Keith haring: a comparison of painting techniques. Microchem. J. 124, 940–948. https://doi.org/10.1016/j.microc.2015.06.003.

La Nasa, J., Campanella, B., Sabatini, F., Rava, A., Shank, W., Lucero-Gomez, P., De Luca, D., Legnaioli, S., Palleschi, V., Colombini, M.P., Degano, I., Modugno, F., 2021. 60 years of street art: a comparative study of the artists' materials through spectroscopic and mass spectrometric approaches. J. Cult. Herit. 48, 129–140. https://doi.org/10.1016/j.culher.2020.11.016.

Lazzari, M., Chiantore, O., 1999. Drying and oxidative degradation of linseed oil. Polym. Degrad. Stab. 65, 303–310. https://doi.org/10.1016/S0141-3910(99)00020-8.

Learner, T., Chiantore, O., Scalarone, D., 2002. Ageing studies of acrylic emulsion paints. In: Vontobel, R. (Ed.), 13th Triennial Metting, Rio de Janeiro, 22-27 September 2002, Prepints, ICOM Committee for Conservation. James & James, London, pp. 911–919.

López, A.J., Ramil, A., Pozo-Antonio, J.S., Rivas, T., Pereira, D., 2019. Ultrafast laser surface texturing: a sustainable tool to modify wettability properties of marble. Sustainability 11, 4079. https://doi.org/10.3390/su11154079.

Marrion, A., 2004. The Chemistry and Physics of Coatings. Published by The Royal Society of Chemistry ISBN 0-85404-656-9. 396p.

Martínez-Cortizas, A., 1987. Zonas agroecológicas de Galicia; zona climática FAO. An Edafol Agrobiol. 46, pp. 521–538.

Martínez-Cortizas, A., Pérez, A., 1999. Atlas climático de Galicia. Consellería de Medioambiente, Xunta de Galicia, p. 210.

Melo, M.J., Bracci, S., Camaiti, M., Chiantore, O., Piancenti, F., 1999. Photodegradation of acrylic resins used in the conservation of stone. Polym. Degrad. Stab. 66, 23–33. https://doi.org/10.1016/S0141-3910(99)00048-8.

Mokrzycki, W., Tatol, M., 2011. Color difference DeltaE-A survey. Mach Graph Vis. 20, 383–411. https://www.researchgate.net/publication/236023905_Color_difference_Delta_E_-_A_survey.

Nguyen, T.B., Hwang, M.-J., Ryu, K.-S., 2012. Synthesis and high photocatalytic activity of zn-doped TiO2 nanoparticles by sol-gel and Ammonia-evaporation method. Bull. Korean Chem. Soc. 33 (1), 243–247. https://doi.org/10.5012/bkcs.2012.33.1.243.

Perrin, F.X., Irigoyen, M., Aragon, E., Vernet, J.L., 2000. Artificial ageing of acrylurethane and alkyd paints: a micro-ATR spectroscopic study. Polym. Degrad. Stab. 70, 469–475. https://doi.org/10.1016/S0141-3910(00)00143-9.

Pintus, V., Wei, S., Schreiner, M., 2016. Accelerated UV ageing studies of acrylic, alkyd, and polyvinyl acetate paints: influence of inorganic pigments. Microchem. J. 124, 949–961. https://doi.org/10.1016/j.microc.2015.07.009.

Ploeger, R., Scalarone, D., Chiantore, O., 2008. The characterization of commercial artists' alkyd paints. J. Cult. Herit. 9 (4), 412–419.

Ploeger, R., Scalarone, D., Chiantore, O., 2009. Thermal analytical study of the oxidative stability of artists' alkyd paints. Polym. Degrad. Stab. 94 (11), 2036–2041.

Pozo-Antonio, J.S., Rivas, T., López, A.J., Fiorucci, M.P., Ramil, A., 2016. Effectiveness of granite cleaning procedures in cultural heritage: a review. Sci. Total Environ. 571. https://doi.org/10.1016/j.scitotenv.2016.07.090.

Rajandas, H., Parimannan, S., Sathasivam, K., Ravichandran, M., Su Yin, L., 2012. A novel FTIR-ATR spectroscopy based technique for the estimation of low-density polyethylene biodegradation. Polym. Test. 31 (8), 1094–1099.

Rivas, T., Pozo, S., Fiorucci, M.P., López, A.J., Ramil, A., 2012. Nd:YVO4 laser removal of graffiti from granite. Influence of paint and rock properties on cleaning efficacy. Appl. Surf. Sci. 263, 563–572. https://doi.org/10.1016/j.apsusc.2012.09.110.

Rivas, T., Pozo, S., Paz, M., 2014. Sulphur and oxygen isotope analysis to identify sources of Sulphur in gypsum-rich black crusts developed on granites. Sci. Total Environ. 482–483, 137–147. https://doi.org/10.1016/j.scitotenv.2014.02.128.

Rivas, T., Pozo-Antonio, J.S., Ramil, A., López, A.J., 2020. Influence of the weathering rate on the response of granite to nanosecond UV laser irradiation. Sci. Total Environ. 706, 135999. https://doi.org/10.1016/j.scitotenv.2019.135999.

Sanmartín, P., Pozo-Antonio, J.S., 2020. Weathering of graffiti spray paint on building stones exposed to different types of UV radiation. Constr. Build. Mater. 236, 117736. https://doi.org/10.1016/j.conbuildmat.2019.117736.

Sanmartín, P., Cappitelli, F., Mitchell, R., 2014. Current methods of graffiti removal: a review. Constr. Build. Mater. 71, 363–374. https://doi.org/10.1016/j.conbuildmat.2014.08.093.

Santos, D.S.S., Korn, M.G.A., Guida, M.A.B., dos Santos, G.L., Lemos, V.A., Teixeira, L.S.G., 2011. Determination of copper, iron, Lead and zinc in gasoline by sequential multi-element flame atomic absorption spectrometry after solid phase extraction. J. Braz. Chem. Soc. 22 (3), 552–557. https://doi.org/10.1590/S0103-50532011000300020.

Saunders, K.J., 1973. Organic Polymer Chemistry. Chapman and Hall, London.

Scalarone, D., Chiantore, O., Learner, T., 2005. Ageing studies of acrylic emulsion paint, part II: comparing formulations with poly (EA-co-MMA) and poly (n-BA-co-MMA) binders. In: Verger, I. (Ed.), 14th Triennial Meeting The Hague, 12-16 September 2005, Prepints, ICOM Committee for Conservation. vol 1. James & James, pp. 350–357.

Socrates, G., 2001. Infrared and Raman Characteristic Group Frequencies: Tables and Charts. third edition. John Wiley and Sons.

UNE-EN 1936:2007, UNE-EN 1936:2007 . Natural Stone Test Methods—Determination of Real Density and Apparent Density, and of Total and Open Porosity.

UNE-EN ISO 4288:1999, 1999. Geometrical Product Specifications (GPS). Surface texture: Profile method, terms, definitions and surface texture parameters.

Vasile, C., 2005. Practical Guide to Polyethylene. RAPRA Technology, Shrewsbury.

Whitmore, P.M., Colaluca, V.G., 1995. The natural and accelerated aging of an acrylic artist's medium. Stud. Conserv. 40 (1), 51–64. https://doi.org/10.2307/1506611.

Xunta de Galicia, 2020. MeteoGalicia. Consellería de Medio Ambiente, Territorio e Vivenda. Xunta de Galicia Accessed 28th September https://www.meteogalicia.gal/web/inicio.action.

Zahner, L.W., 2019. Aluminum Surfaces: A Guide to Alloys, Finishes, Fabrication and Maintenance in Architecture and Art. John Wiley & Sons 400 pp.

Zhang, M., Feng, S., Wang, L., Zheng, Y., 2016. Lotus effect in wetting and self-cleaning. Biotribology 5, 31–43.